A

Thesis on

Particle size influenced multiferroic properties of Eu doped $BiFeO_3$

Dissertation submitted in partial fulfilment for the requirement of the award of the degree of

Master of Science

in

Physics

Under

The supervision of

Dr. Poonam Uniyal

(Associate Professor)

Submitted by

Gulshan Dhillon

Roll no: - 301504012

School of Physics and Materials Science

Thapar University

Patiala (Punjab) – 147004

July, 2017

Dedicated to my parents….

Certificate

This is to certify that the thesis entitled "Particle size influenced multiferroic properties of Eu doped $BiFeO_3$" submitted by **Ms.Gulshan Dhillon** in the partial fulfillment of the requirement for the award of the degree of Master of Science in Physics from the School of Physics and Materials Science, Thapar University, Patiala, is an authentic record of his own work carried out under the supervision and guidance of **Dr. Poonam Uniyal**. The matter embodied in this report is one of the candidate's own record and not submitted to any other university in any part or full form for the award of such kind of degree.

Gulshan Dhillon

Dr. Poonam Uniyal

Supervisor

(Associate professor)

School of Physics and Materials Science

Thapar University

Patiala, Punjab

Acknowledgement

First of all I would like to extend my gratitude towards my supervisor, Dr. Poonam Uniyal (Associate Professor), School of Physics and Materials Science, Thapar University, Patiala, for giving me a chance to work in her supervision and without her help & constant guidance this thesis would have not completed.

I wish my sincere thanks to Dr. Manoj Kumar (Professor and Head), School of Physics and Materials Science, Thapar University, Patiala for their support and encouragement

I would like to give my sincere regard for all the faculty members and technical staff in School of Physics and Materials Science, Thapar University.

I would like to thank Dr. K.L. Yadav (Professor, IIT Roorkee) for their kind help in carrying out some experimental work.

In particular I am very thankful to Dr. Gitanjali Dhir, Mrs. Manpreet Kaur Sharma and Dr. Nanda Shakti for helping me in experiments and giving me moral support.

No words can explain my gratitude to my parents and brother whose blessings and support have shown me the path to pursue my goal in life.

Gulshan Dhillon

List of Figures and Tables

Fig.1.1 Types of ferroic materials

Fig.1.2 Multiferroic and magnetoelectric relationship

Fig.1.3 View of pervoskite structure

Fig.1.4 Geometric mechanism of polarization generation in $YMnO_3$

Fig.1.5 Polarization caused due to ordering of Bi^{3+} ion in $BiFeO_3$.

Fig.1.6 $PbTiO_3$ has rhombohedrally distorted structure

Fig.1.7 Pervoskite structure of $BiFeO_3$

Fig.1.8 G type antiferromagnetism of $BiFeO_3$

Fig.2.1 Common synthesis techniques for bismuth ferrite

Fig.2.2 Preparation technique of pure Bismuth Ferrite

Fig.2.3 Preparation technique of Europium doped Bismuth ferrite

Fig.2.4 Schematic for Bragg's Law

Fig.2.5 PANalytical's X-ray diffractometer

Fig.2.6 Working diagram of SEM

Fig. 2.7 M-H hysteresis loop of soft and hard metals

Fig.3.1 (a)XRD patterns of synthesized pure bismuth ferrite,Eu doped BFO at vaying calcination temperatures of 450° C,550° C,650° C.

(b) Enlarged view of most intense peak of the synthesized nano-particles

(c) Williamson Hall plot of BFO

(d) Williamson Hall plot of Eu-BFO(450°C)

(e) Williamson Hall plot of Eu-BFO(550°C)

(f) Williamson Hall plot of Eu-BFO(650°C)

Fig.3.2 (a) FE-SEM image of BFO

(b) FE-SEM image of Eu-BFO (450° C)

(c) FE-SEM image of Eu-BFO (650° C)

Fig.3.3 (a) M-H loops of synthesized nanoparticles at various calcination temperatures.

(b) Enlarged view of M-H hysteresis loop of BFO with positive and negative coercive fields.

(c)) Enlarged view of M-H hysteresis loop of Eu-BFO(450° C) with positive and negative coercive fields.

(d)) Enlarged view of M-H hysteresis loop of Eu-BFO(550°C) with positive and negative coercive fields.

(e)) Enlarged view of M-H hysteresis loop of Eu-BFO(650°C) with positive and negative coercive fields.

Fig.3.4 (a) Frequency dependence plot of dielectric constant

(b) Dielectric loss of BFO, Eu-BFO(450°C),Eu-BFO(650°C)

Table 3.1 Values of lattice parameters, volume and crystallite size of synthesized samples

Table 3.2 Calculated Values of M_s and M_r of synthesized nanoparticles

List of Symbols

θ	Angle
A	Area
C	Curie constant
T_C	Curie temperature
K	Kelvin temperature
d	Interplanar distance
n	Integer
P	Polarization
ε	Permittivity of material
ε_o	Permittivity of vacuum
P_r	Remnant polarization
ε_r	Relative permittivity
P_s	Spontaneous polarization
P_{sat}	Saturation value
T	Temperature
t	Thickness
λ	Wavelength
M	Magnetization
H	Applied magnetic field
α	Angle (lattice parameter)
Å	Angstrom
μ	Micron
β	Full width at half maxima
T_N	Néel temperature

Abstract

A study has been done to investigate the effect of Europium doping and crystallite size on the multiferroic properties of $Bi_{(1-x)}Eu_xFeO_3$ (x=0,0.15) nanoparticles. Crystallite size of Europium doped nanoparticles was altered by changing their calcination temperatures. Europium doping resulted in structural change from rhombohedral to orthorhombic. Enhanced magnetization has been observed in the Eu^{3+} doped nanoparticles which further reduced with increment in particle size. Improvement in dielectric properties was also witnessed with Eu^{3+} substitution. Hence, study represents a relationship among multiferroism, ionic substitution and particle size.

Table of contents

Certificate [iii]
Acknowledgement [iv]
List of Figures and Tables [v]
List of symbols [vii]
Abstract [viii]

Chapter-1 INTRODUCTION

1.1 History 1
1.2 Introduction 1
1.3 Multi ferroics 2
1.4 Types of Multiferroics 2
1.5 Bismuth Ferrite 4
1.6 Crystal structure of BFO 5
1.7 Applications of Bismuth Ferrite 6
1.8 Literature Review 7
1.9 Motivation for the work 9

Chapter- 2 SYNTHESIS AND CHARACTERIZATIONS

2.1 Synthesis 10
2.1.1 Sol Gel Method 10
2.2 Charcterization techniques 12
2.2.1 X- Ray Diffraction 12
2.2.2 Scanning Electron Microscopy 14
2.2.3 Vibrating Sample Magnetometry 14
2.3.4 Dilectric measurement 15

Chapter- 3 RESULTS AND DISCUSSION

3.1 Structural Analysis 16
3.2 Microstructural Analysis 20
3.3 Magnetic Analysis 22
3.4 Dilectric Analysis 25

Conclusion 28

Refrences 29

1.1 HISTORY

The coexistence of electricity and magnetism has been a topic of great interest for researchers since last few decades. In 1820, Hans Christian Oersted observed that by switching the current on or off in the nearby battery, compass needle deflected. This observation was later studied by Ampere, Andre Marie and Michael Faraday.In 1860, James Maxwell gave his equations clubbing together magnetism and electricity in similar conditions which were earlier considered to be separate.

1.2 INTRODUCTION

Different materials have different properties which are categorised as electrical, magnetic, dielectric, optical etc. Materials which adopt a switchable, spontaneous internal alignment are defined as ferroics[1]. Types of ferroic materials are:

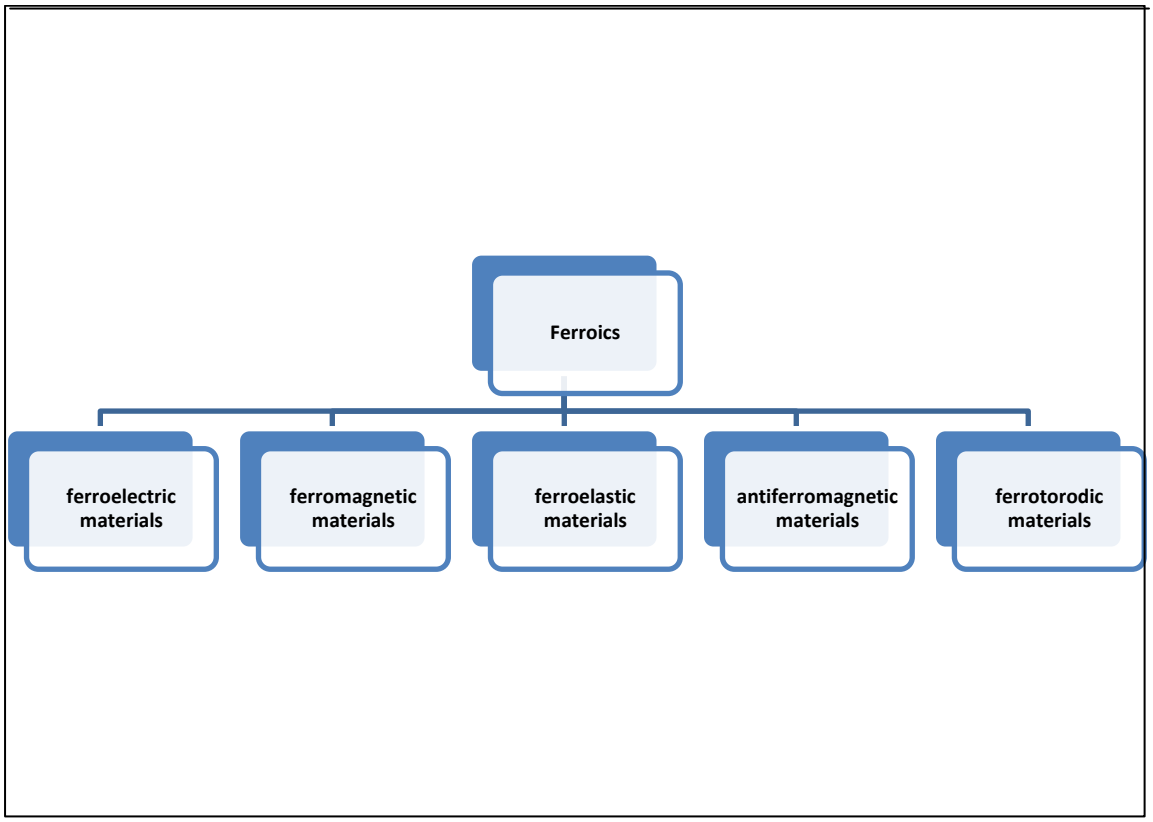

Fig.1.1 Types of ferroic materials

1.3 Multiferroics

Multiferroics are the materials that exhibit simultaneous presence of two or more primary ferroic order parameters such as ferroelectricity, farromagneticity, ferroelasticity in one phase.

The coupling between ferroelectric and ferromagnetic interactions results in magneto electric (ME) effect. The simultaneous existence of ferroelectric and ferromagnetic orders is a essential for a material to be categorised as magneto electric material.

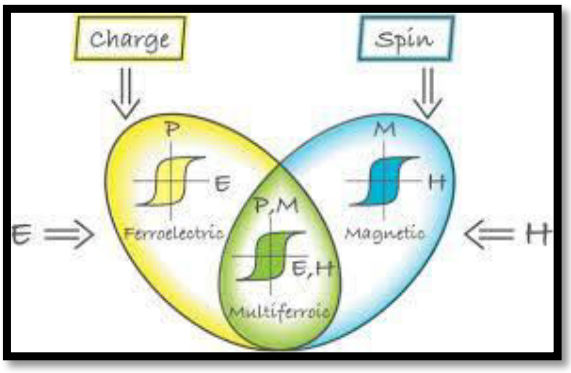

Fig.1.2 Multiferroic and magnetoelectric relationship

The multiferroic and magnetoelectric relationship is shown diagrammatically in fig.1.2. The figure shows that ferromagnetic(ferroelectric) materials are a subset of magnetically(electrically) polarizable materials. The intersection between them represent multiferroic materials.

1.4 Types of multiferroics

Mutltiferroics are divided into following two categories[2].

1. Mutiferroics- Type 1

2. Multiferroics- Type 2

TYPE 1 MULTIFERROICS: The source of magnetism and ferroelectricity are different in these types of mutliferroics which appear to be largely independent of each other but they have some coupling between them. Magnetic and ferroelectric coupling in such kind of materials is generally weaker. These materials show ferroelectricity at higher temperature than magnetism and their spontaneous polarization has larger value.

Examples include Bismuth ferrite($BiFeO_3$), $YMnO_3$.

Major subclasses of type 1 multiferroics are:

- *Multiferroics with pervoskite structure*: These compounds have general formula ABO_3 or $A_2B´B´´O_6$. The partially filled d-shells of transition metals are essential for magnetism in such systems and the ferroelectricity is produced due to the off-centre shifts of transition metal ions, which are covalently bonded with one or three oxygen atoms, with the use of their empty d states. Examples are $BaTiO_3$, $Pb(ZrTi)O_3$.

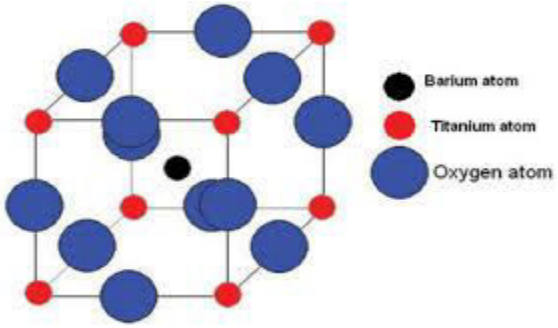

Fig.1.3 :View of pervoskite structure

- *Geometric ferroelectricity*: Ferroelectricity in $YMnO_3$[3] is generated due to the tilting of rigid MnO_3 with magnetically active Mn residing at the centre. This titling makes denser packing available due to which oxygen ions move close to smaller Y ions.

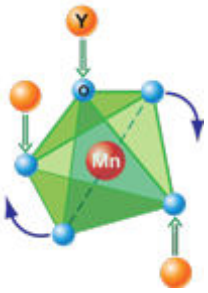

Fig.1.4 Geometric mechanism of polarization generation in $YMnO_3$ [3]

- *Multiferroic behaviour due to lone pair:* The materials which show such type of multiferroicity are $BiFeO_3$, and also probably in $BiMnO_3$ and PVO_3 where ferroelectricity is caused due to Bi^{3+} and Pb^{3+}. The 6s electrons present in these ions do not form bonds. Due to this, high polarizability is caused which is the required condition for ferroelectricity. The alignment of lone pairs in one direction generates ferroelectricity as well as improves it.

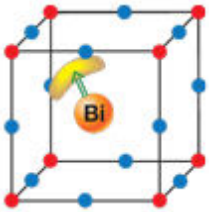

Fig.1.5 Polarization caused due to ordering of Bi^{3+} ion in $BiFeO_3$.

- *Charge ordered Multiferroics:* This kind of multiferroicity is usually seen in those transition metal compounds which have transition metal ions of variable valency.

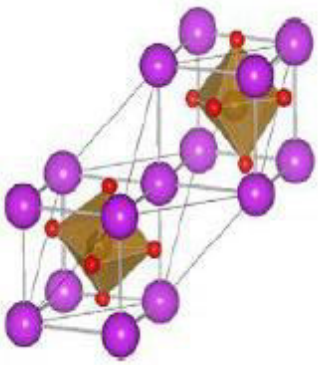

Fig.1.6 $PbTiO_3$ has rhombohedrally distorted structure

TYPE-2 MULTIFERROICS: In these materials, ferroelectricity is produced by a special kind of magnetism[4,5].Smaller value of polarization is experienced in these materials.(~10μC/cm^2).Examples are: $TbMnO_3$, $TbMn_2O_5$.Multiferroics of type 2 are further divided into following categories:

- *Multiferroics of type 2 spiral:* In such Multiferroics, ferroelectricity occurs along with spiralling magnetic phase, usually of cycloid type.
- *Collinear magnetic structures Multiferroics of type 2*: In these Multiferroics, ferroelectricity occurs in collinear magnetic structures.

Among multi-ferroics, Bismuth ferrite has gained large attention due to its high ferroic ordering temperatures and relatively simple structure.

Bismuth Ferrite

Bismuth ferrite($BiFeO_3$) exhibits multiferroic properties at room temperature and is one of the most promising lead free piezoelectric material. It is always considered to be

antiferromagnetic in its bulk form, having antiferromagnetic Néel temperature of T_N=643K and ferroelectric curie temperature of T_C=1103K. Bi^{3+} and Fe^{3+} ions are considered responsible to produce ferroelectricity and magnetism respectively.In bulk form, $BiFeO_3$ can be explained as rhombohedrally distorted ferroelectric pervoskite with R3c space group. Spontaneous polarization is caused along pseudo cubic[111] direction in distorted structure. Since each Fe^{3+} is surrounded by six nearest Fe neighbours of antiparallel spin, therefore, it is G-type antiferromagnetic.

1.6 Crystal Structure of Bismuth Ferrite

- At room remperature, bismuth ferrite has rhombohedrally distorted structure along with R3c space group.

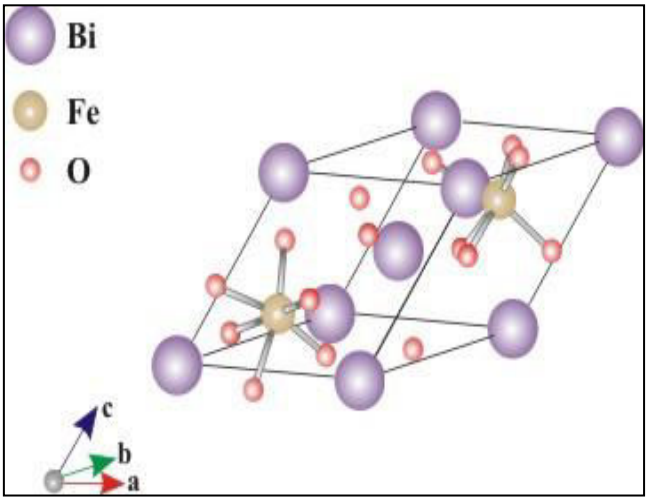

Fig.1.7 Pervoskite structure of $BiFeO_3$

- Corners are occupied by Bi^{3+} ions, Fe^{3+} ion has body centeral position whereas O^{2-} ions are located at face centered position. The corresponding lattice parameters of BFO are a=5.587 Å, b=5.587 Å and c=13.867 Å along with the lattice angles $\alpha = \beta = 90°$ and $\gamma = 120°$.

Ferroelectricity is generally caused due to empty d^0 orbital whereas ferromagnetism is caused because d^n orbital which is not completely filled. Stereo-chemical behaviour of Bi^{3+} ion produces ferroelectricity whereas Fe^{3+} ion produces ferromagnetism. [6]

DIELECTRIC CONSTANT:

At room temperature the dielectric constant of BFO is ε_r =30 [20,21,22,23] at GHz frequencies. Due to ferroelectric-paraelectric transition, the dielectric constant value peaks at

rhombohedral-orthorhombic transition at 825-840°C. Compared to those of typical pervoskite ferroelectrics, BFO has a smaller value of dielectric constant.

MAGNETISM:

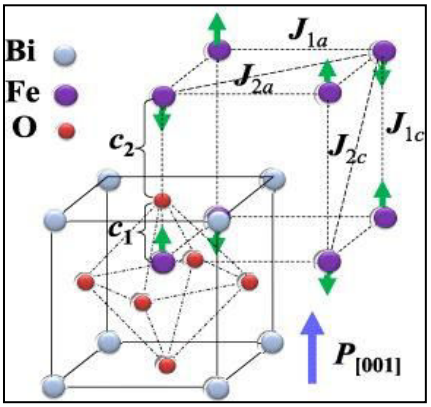

Fig.1.8 G type antiferromagnetism of $BiFeO_3$

Each Fe^{3+} spin is surrounded by six antiparallel spins on the nearest Fe neighbour, that is, G-type antiferromagnetism. the spins are not perfectly anti-parallel because local magnetoelectric coupling causes weak canting moment. Moreover, superimposed over canting moment, there is another long range super structure containing an incommensurate cycloidal spin structure of anti-ferromagnetically ordered sub lattices along [1 1 0] direction.

FERROELECTRICITY:

- *BULK*: BFO is room temperature multiferroic in its bulk form having spontaneous electric polarization directed along one of the [1 1 1] direction of pervoskite.the ferroelectric polarization of bismuth ferrite being oriented to <111> direction leads to the production of 8 possible polarization direction.

1.7 APPLICATIONS OF BISMUTH FERRITE[7]:

1. Bismuth Ferrite is widely used in field of transducers, information storage devices, magnetic field sensors etc. due to its multiferroic behaviour.

2. Ferroelectric random access memories(FeRAMs) have achieved high densities(64 Mb), fast access speeds (5ns) in the recent times.

3. BFO has applications in low power consumption, fast , multifunctional memory devices. Due to the magnetoelectric coupling present in BFO, data can br written electrically and read magnetically.

1.8 LITERATURE REVIEW:

Although the existence of ferroelectric and magnetic orders in a single phase, in BFO make it unique but it has low magnetoelectric coupling values, weak magnetism and high leakage current density[8]. Reduction in particle size has resulted in enhancement of multiferroism.[9-13].

Gitanjali Dhir *et al.* [14] used sol gel method to synthesize pure and Tb doped BFO samples. Orthorhombic phase in Bismuth ferrite was also revealed by Tb doping which enhanced its magnetic and ferroelectric properties. The saturation magnetization value(M_S) was enhanced to 3.1221 emu/g by reducing the particle size of Tb doped BFO to 12.7nm. Ratio of surface to volume increases when particle size is reduced and so is uncompensated spin's contribution.

Mehedi Hasan *et al.* [15] synthesized $Bi_{0.9}\ Ba_{0.1}\ FeO_3$ nanoparticles with size ranging from ~ 12 to 49 nm. It was observed that particles with size less than 23nm had almost negligible coercivity whereas the saturation magnetization enhanced largely in ~12 nm $Bi_{0.9}\ Ba_{0.1}\ FeO_3$ nanoparticles. This enhancement is possibly because of combined effect of size confinement and substitution of cation. Improved electrical properties in doped nanoparticles were observed compared to undoped samples.

Manpreet kaur *et al.* [16] studied the multiferroic and optical properties of $Bi_{0.9}Ba_{0.1}Fe_{0.8}Ti_{0.2}O_3$ nanoparticles synthesized using the method of sol gel. The particle size was in 10-15nm range which exhibited tetragonal structure *P4m.* Band gap of 2.161 eV was measured by UV-visible absorption method. RB-5 dye vanished upto 94% which revealed that the synthesized nano particles were proficient photocatalytic semiconductor for the degradation of dye.

There is a strong dependency of Néel temperature on particle size. Z.M. Tian *et al.* synthesised $Bi_2Fe_4O_9$ ceramics by modified Pechini method and observed that Néel temperature of polycrystalline $Bi_2Fe_4O_9$ samples decreases to 229K as the particle size of the samples becomes 60nm.[17]

Jian Liu *et al.* [18] studied the effect of Europium doping on bismuth ferrite nanoparticles. BEFO samples showed an increase in magnetization with increase in Eu^{3+} concentration. This may be due to the appearance of europium orthoferrite at BEFO $_{x=0.15}$. They also stated that Eu^{3+} ions had more effect in increasing the value of MR in comparison to other RE ions. such as La^{3+}, Nd^{3+}, or Sm^{3+}.

Sunil Chauhan *et al.* [19] prepared pure bismuth ferrite along with $Bi_{0.85}A_{0.15}FeO_3$ (A= Ba, Sr and Ca) nanoparticles by sol gel method. XRD studies revealed that the double split peaks obtained for pure BFO and Ba, Sr doped BFO samples at 2θ~32° which merged into single peak with Ca doping. It is possibly due to the heterovalent ionic size variation which generated lattice distortion. The band gap values obtained were 2.12,2.06, 2.10 and 2.03 eV for pure bismuth ferrite, $Bi_{0.85}Sr_{0.15}FeO_3$, $Bi_{0.85}Ca_{0.15}FeO_3$ and $Bi_{0.85}Ba_{0.15}FeO_3$ nano particles. This indicated that the band gap of bismuth can be altered by heterovalent ions doping.

Gitanjali Dhir *et al.* [20] studied the effect of rare earth doping on barium ferrite. $Bi_{1-x}Dy_xFeO_3$ nanoparticles were prepared using sol gel method. Double peaks of BFO round $2\theta \approx 32°$ are seen merging into single peak with Dy^{3+} ions doping which is an indication of structural transformation from rhombohedral to orthorhombic. This is so because Dy^{3+} ions with smaller ionic radius when replace the larger atomic radius Bi^{3+} ions, the tolerance factor decreases and this causes compression amongst Fe-O bonds.

Wanwan Meng *et al.* [21]synthesized BFO and $Bi_{1-x}La_xFeO_3$ (x =0.10, 0.15, 0.20) samples to study the influence of lanthanum doping on photocatalytic properties of bismuth ferrite. The band gap values were found to decrease from 2.10 eV to 2.07 eV when the concentration of lanthanum doping was increased. Further it was observed that photoctalytic degradation of phenol increased largely upto 96% with 15% La-doped Bismuth Ferrite.

Devender Jalandhara *et al.* [22] prepared bismuth ferrite nano particles via sol-gel method and studied the effect of sintering temperature on particles. It was observed that particle size increased from 37nm to 51nm with increase in temperature from 600° C to 850° C. Optical studies revealed that band gap increased upto 2.54 eV. Hence, it resulted in reduction of refractive index due to the increased band gap.

1.9 Motivation for the work

Doping of different elements in the periodic table enhance properties of BFO such as ferroelectric properties, remanent magnetization, leakage current [23-26]

The doping effect of different elements on -bismuth ferrite are discussed below:

- TRANSITION METALS: These are usually paramagnetic ions due to unpaired electrons. They have 2 or more oxidation states usually differing by one. These metals enhance the ferroelectric and leakage current properties of bismuth ferrite. For eg. Mangenese, cobalt.
- ALKALINE EARTH METALS: The doping of alkaline earth metals into bismuth ferrite increases the band gap which ultimately increases the resistivity and multiferroic behaviour of BFO. For eg. Calcium, magnesium.
- RARE EARTH METALS: These elements are found in group 3 of the periodic table. Their ions possess an oxidation state of +3, except Eu^{2+} and Ce^{4+}. Doping of these ions improves the remanent magnetization because of the suppression of spin spiral structure of bismuth ferrite.

Having learnt the effect of rare earth doping on bismuth ferrite we were motivated to use rare earth as a dopant in the study. Out of the various rare earth metals, Europium was made a choice due to the following reasons:

- Eu^{3+} ion is expected to induce larger distortions to structure of bismuth ferrite as it has smaller ionic radii (1.07Å) than other reported rare earth ions,
- Eu^{3+} being magnetically active is expected to couple with Fe^{3+} ions which causes ferromagnetic ordering and hence enhances the magnetization of BFO even at very low doping concentrations.

It has been concluded from various studies that particle size has a significant role in determining properties of bismuth ferrite[12-14]. Although the doping effect of Europium on bismuth ferrite has been studied earlier but to the best of our knowledge the simultaneous effect of Europium doping along with particle size has not been studied enough. Hence, keeping this fact in mind we studied the behaviour of bismuth ferrite on europium doping simultaneously with the particle size effect.

2.1 SYNTHESIS TECHNIQUE:

The various methods which are usually used the preparation of $BiFeO_3$ are:

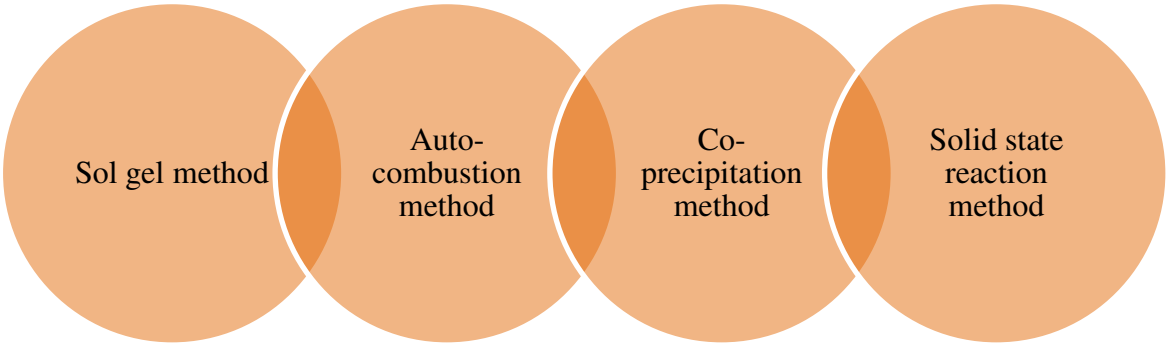

Fig.2.1 Common synthesis techniques for bismuth ferrite

2.1.1Sol gel method

This process can be defined as: "Formation of an oxide network via polycondensation reactions of a molecular precursor in some liquid." A sol can be described as the stable dispersion of colloidal polymers or particles in a solvent[23]. Gel contains a 3-D regular network, that encloses a dilute phase.Usually, the sol particles interact by van der Waals forces. A gel can also be formed by linking polymer chains.Mostly, in gel systems that are practised for the synthesis of materials, the gelation process is irreversible and the interactions are of covalent nature. If other interactions are involved, then the gelation may be reversible. The main idea behind sol-gel synthesis is to "dissolve" the compound in a liquid so that it could be brought back to solid in a controlled manner. Various advantages of sol gel method are:

•Multi component compounds can be synthesized by controlled stoichiometry in which sols of different compounds are mixed.

•It prevents co-precipitation problems.

•Easily sinterable small particles are formed.

In the present work, all the samples are prepared by sol gel method. The flowchart for the prepration of pure $BiFeO_3$ nanoparticles is given below:

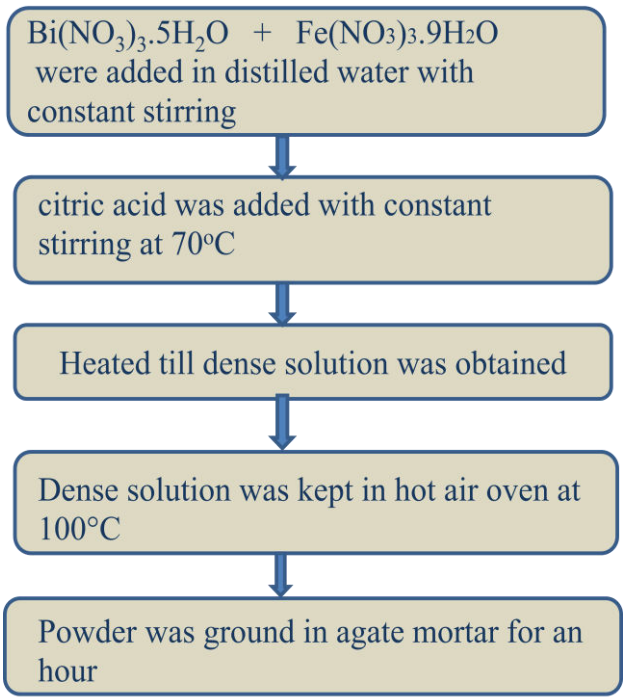

Fig.2.2 Preparation technique of pure Bismuth Ferrite

The powder thus obtained was calcined at 450°C in muffle furnace. The prepared sample was named as BFO. $Bi_{(1-x)}Eu_xFeO_3$ (x=0.15) samples were prepared with the following steps:

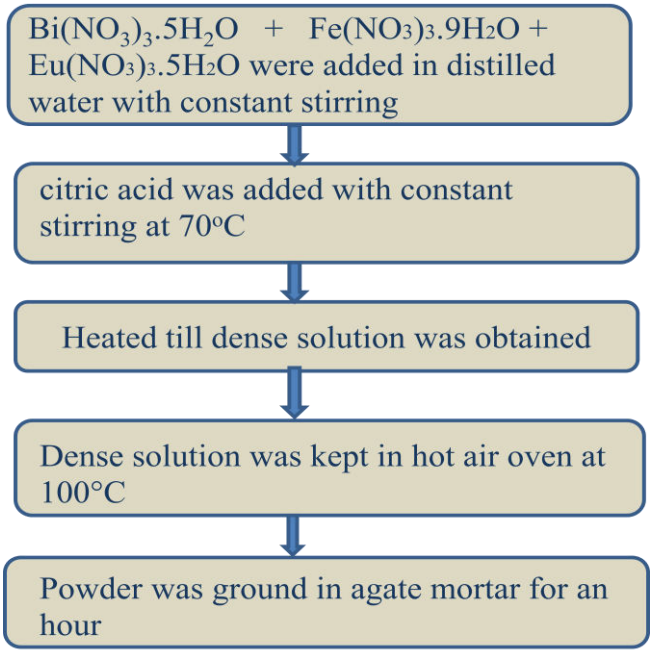

Fig.2.3 Preparation technique of Europium doped Bismuth ferrite

The powder thus obtained was calcined at separate temperatures of 450°C,550°C and 650°C to alter the particle size of the synthesized samples. The nanoparticles obtained were named as Eu-BFO(450°C),Eu-BFO(550°C),Eu-BFO(650°C) respectively.

2.2 Characterization Techniques

2.2.1 X-ray diffraction(XRD)

X-ray powder diffraction is an important method to study the complete picture regarding crystallographic and chemical behaviour of the materials. It can identify the materials that are not known and dimensional information on unit cell can also be provided by it.

Principle of X-Ray Diffraction

In XRD experiments, a focused beam of X-rays is made to strike the sample. Generally, crystal diffracts the X-ray beam uniquely, depending on its orientation as well as structure. An area detector collects the diffracted X-ray. Reflections of different intensities form the diffraction pattern which help in determining the structure of the crystal. However, before identifying the true crystal structure, certain orientations of the crystal should be collected.

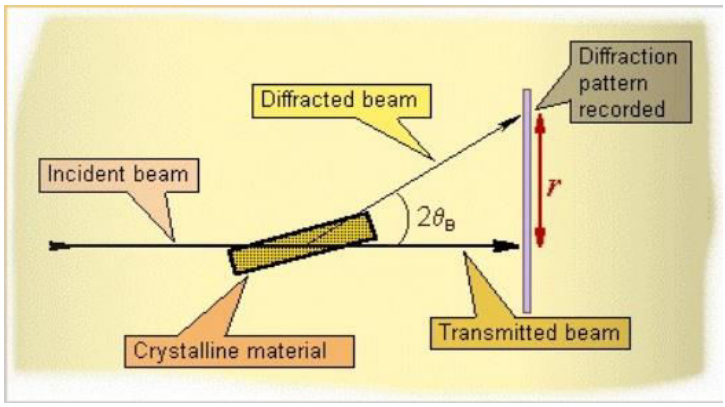

Fig.2.4 Schematic for Bragg's Law

It basically works on the principle of Bragg's Law which states that:

$$2dsin\theta = n\lambda \qquad (2.1)$$

Where, n is an integer, λ is the wavelength of x-rays,d is the spacing between the planes and θ is the angle between the scattering planes and the incident rays.

The instrument used for XRD is shown:

Fig.2.5 PANalytical's X-ray diffractometer

2.2.2 SCANNING ELECTRON MICROSCOPY(SEM):

Electron column, EDS detector, monitors, sample chamber and electronics console are the main components of a SEM instrument. Various signals are generated at the surface of samples using focused beam of electrons having high energy.

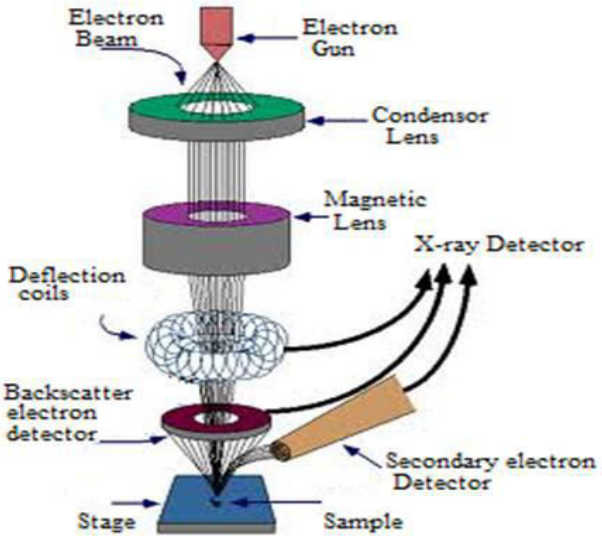

Fig.2.6 Working diagram of SEM

The interactions between the electron beam and sample generate the patterns which reveal details about the sample including orientation, crystallinity, external texture, and chemical compositions that build up the material.

2.2.3 VIBRATING SAMPLE MAGNETOMETRY(VSM):

A vibrating sample magnetometer is an instrument which measures the magnetic properties of material. The vibrating component produces variation in the magnetic field of the material, which gives rise to an electrical field in the coil. It is based on Faraday's Law of Induction. During VSM, the material is kept within sensing coils, also held at the desired angle. The vibrating sample is made to go through sinusoidal motion, i.e., mechanically vibrated.

The values obtained by the software when observed graphically give us the hysteresis loop.

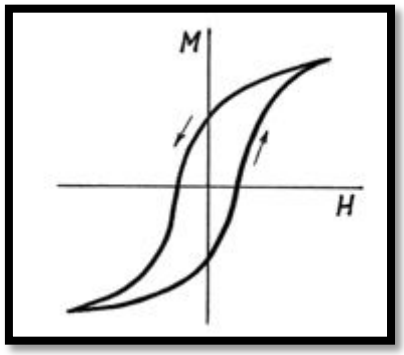

Fig.2.8 M-H hysteresis loop

The hysteresis loop visualize the "history dependent" behaviour of magnetization of a ferromagnetic material. Once the saturation has been derived by the material, the magnetizing field can then be dropped to zero and the material will retain most of its magnetization.

2.2.4 DIELECTRIC MEASUREMENT:

LCR meter is an electronic equipment that measures the inductance(L), capacitance(C) and resistance(R) of a material. These quantities are determined from the measurement of impedance. The required calculations are incorporated in device's circuitry; where meter reads L, R and C directly. It allows testing of materials up to 1 MHz and provides a built-in contact check for good connection. Due to these capabilities, handling a variety of components is more realistic for test conditions.

3.1 STRUCTURAL PROPERTIES:

Fig. 3.1(a) shows the XRD plotting of all the peaks associated with undoped Bismuth ferrite correspond to rhombohedral structure (Reference card no.-01-074-2016). A double splited peak is obtained at 2θ~32°. Due to chemical kinetics of formation, secondary phases are obtained as minor phase with $BiFeO_3$ which leads to the formation of some impurity peaks at 2θ~28° marked as * in fig.3.1(a). This peak corresponding to $Bi_{24}Fe_2O_{39}$ is not ferromagnetic at room temperature and hence does not contribute to magnetism.[22].

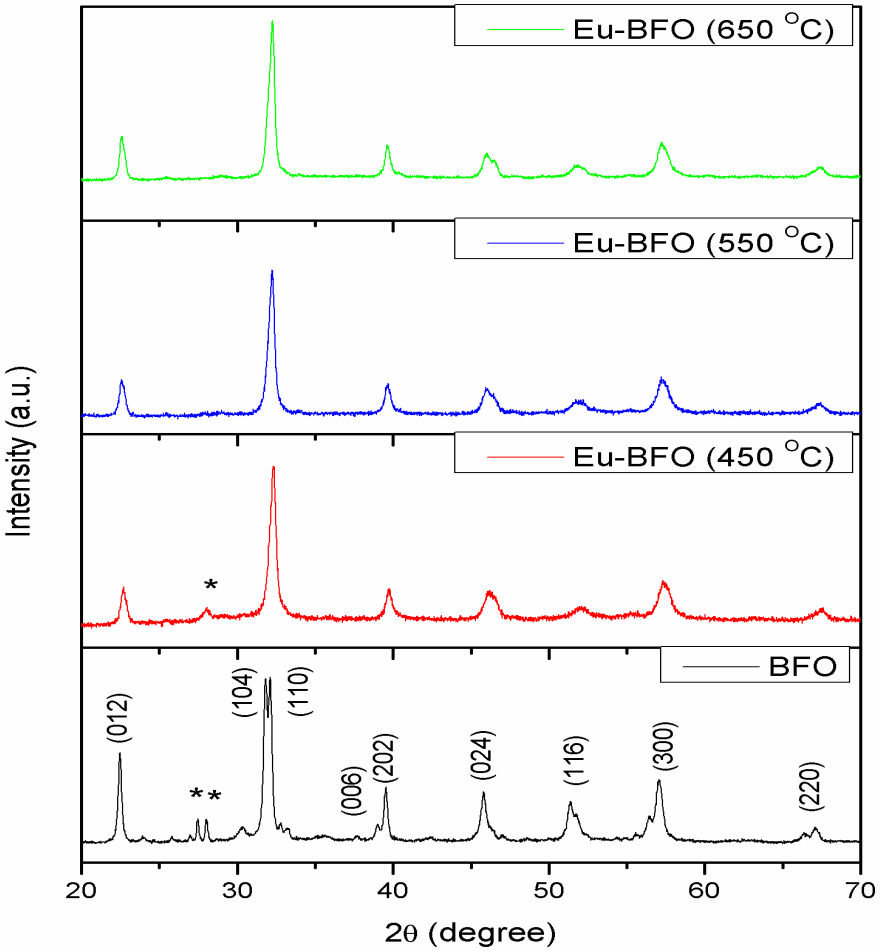

Fig.3.1(a) XRD patterns of BFO, Eu-BFO(450°C),Eu-BFO(550°C) and Eu-BFO(650°C) nanoparticles.

Europium doping resulted in few notable changes as depicted in fig.3.1(b). It revealed that the two Distinctive reflection peaks merged into a single peak and also shifted towards higher value of 2θ. It indicates that the structural transformation has been induced by Eu ions substitution. This shift itself is a proof that Eu^{3+} ions have been substituted at place of Bi^{3+} ions in the lattice. This confirms the change in rhombohedral structure of BFO to

orthorhombic structure due to Eu doping in the BFO lattice. The peaks of Eu doped nanoparticles are well matched with JCPDS card no.-00-046-0134. Further, with increase in calcination temperature of Europium doped nanoparticles the peaks shifted towards lower values of 2θ. Impurity peaks also diminished as the calcination temperature of the synthesized nanoparticles was increased.

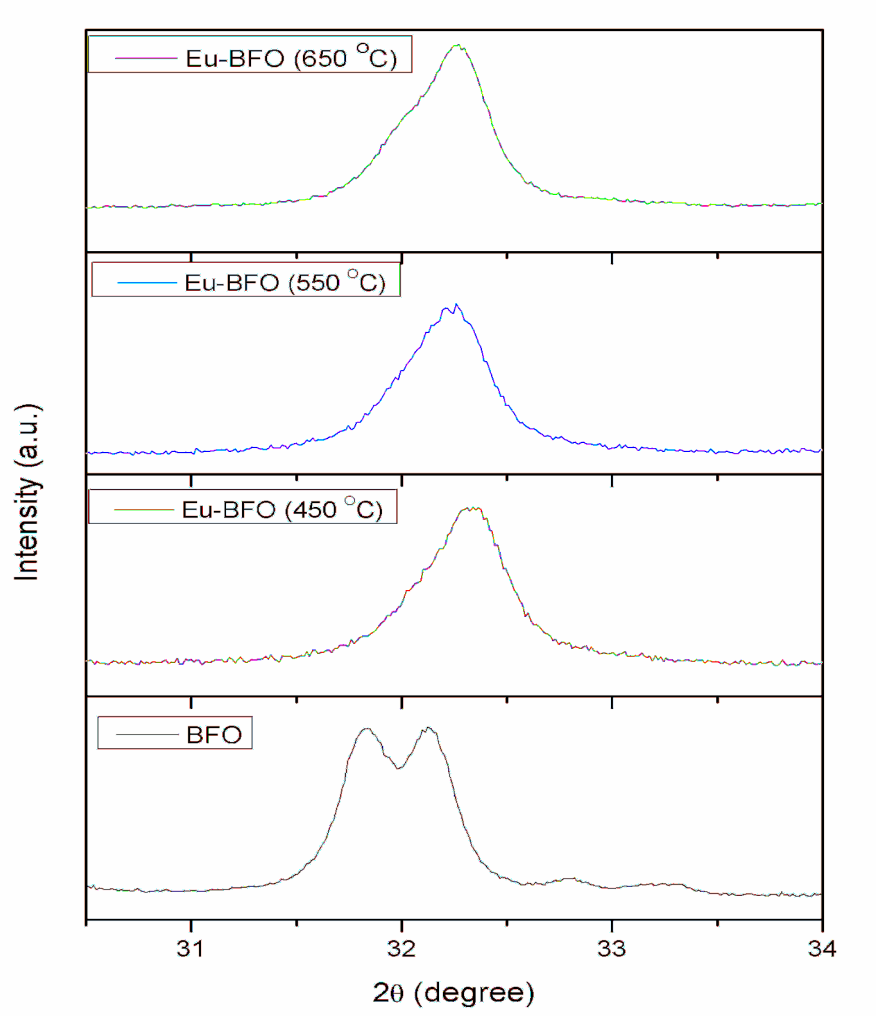

Fig.3.1(b) Enlarged view of most intense peak of the synthesized nano-particles.

Shifting of peaks clearly means that the lattice parameters have been altered. The calculated values of lattice parameters for different synthesized nanoparticles have been listed in table 1. The average particle size has been calculated by using Williamson Hall Method and the instrumental broadening (hkl) was corrected, corresponding to each diffraction peak of $BiFeO_3$ nanoparticles using the below relation:

$$\beta_{hkl} = \left[\left(\beta_{(meas.)hkl}{}^2\right) - \left(\beta_{(inst.)hkl}{}^2\right)\right]^{1/2} \qquad (3.1)$$

And the Williamson Hall equation is of the form[27]:

$$\beta_{hkl}\, cos\theta_{hkl} = \left[\frac{k\lambda}{D}\right] + [4\varepsilon sin\theta_{hkl}] \tag{3.2}$$

Where λ=wavelength of incident rays, k= shape factor(0.9), D= crystallite size,

θ= Bragg's angle and ε= strain induced.

The crystallite size was calculated from the intercept of line plotted between 4$sin\theta$hkl and $\beta cos\theta hkl$. The linear equation used for the curve fitting was:

$$y = a + bx \tag{3.3}$$

Where *a,b* are variables and *x* is constant.

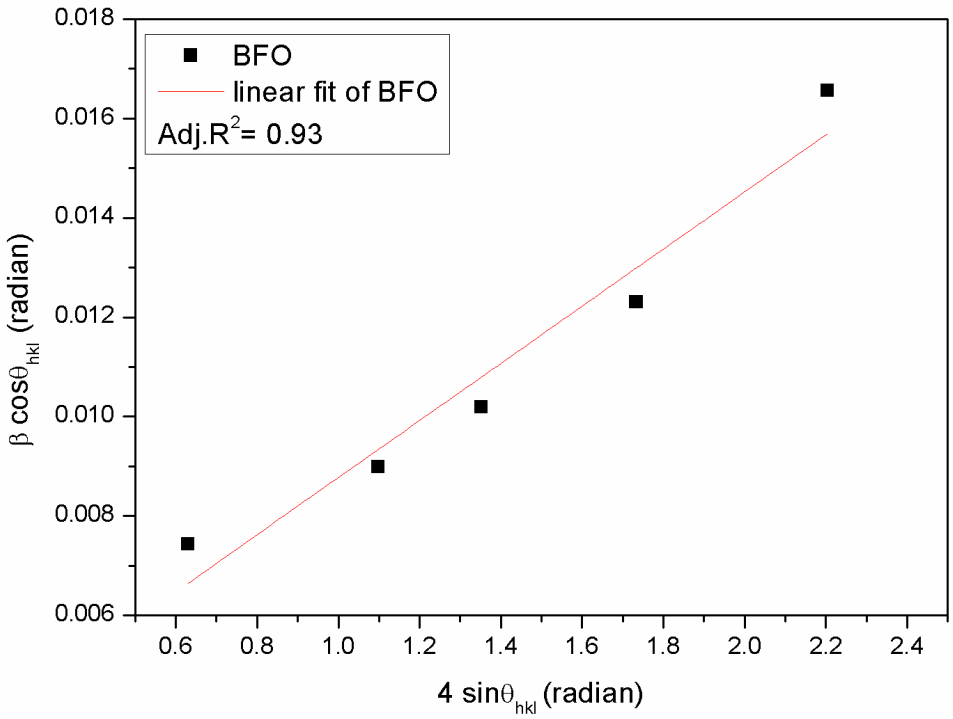

Fig.3.1(c) Williamson Hall plot of BFO

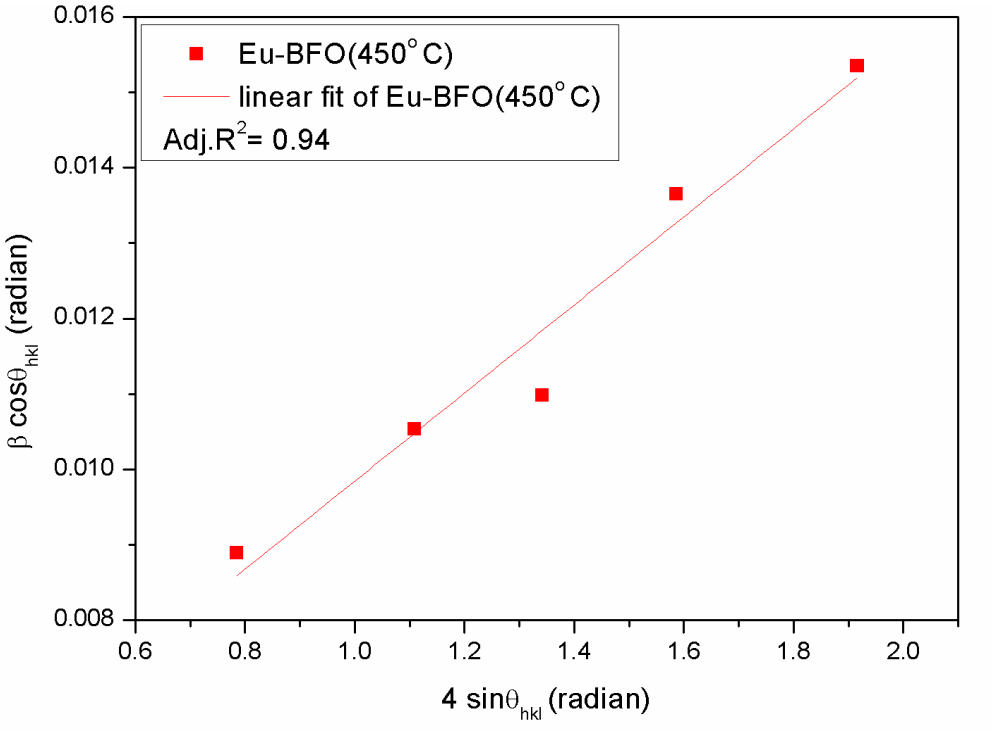

Fig.3.3(d) Williamson Hall plot of Eu-BFO(450°C)

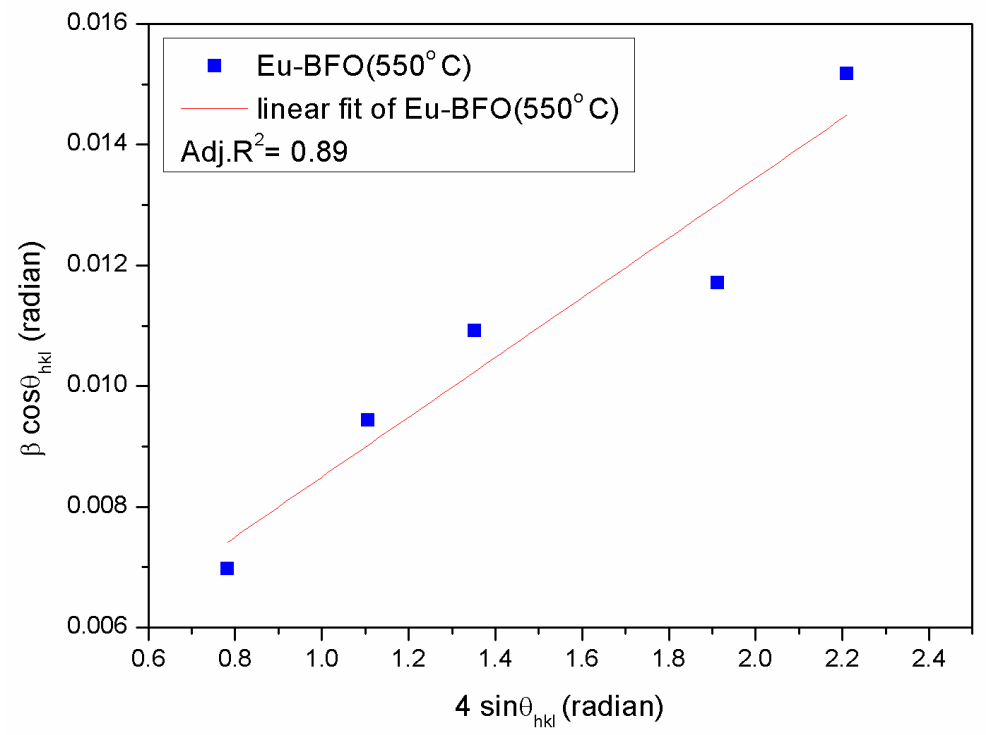

Fig.3.1(e) Williamson Hall plot of Eu-BFO(550°C)

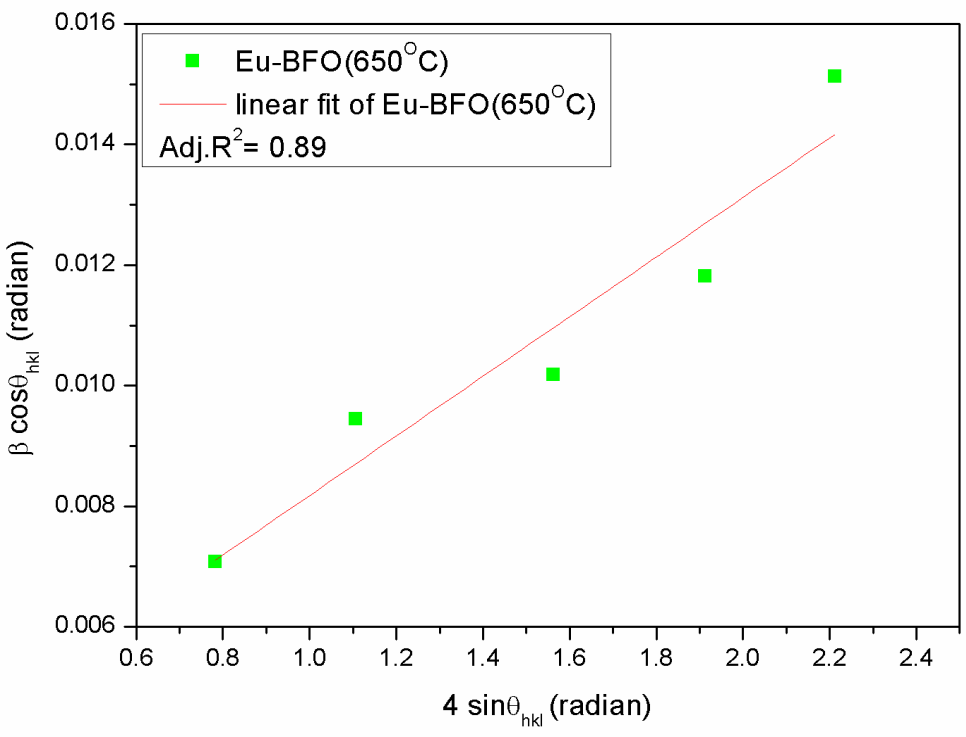

Fig.3.1(f) Williamson Hall plot of Eu-BFO(650°C)

From the intercept values of the plot lines, the crystallite sizes of different samples were calculated. The lattice parameters have been calculated using the below mentioned formulas for different structures possessed by the nanoparticles:

$$\frac{1}{d^2} = \frac{4}{3}\left(\frac{h^2+hk+k^2}{a^2}\right) + \frac{l^2}{c^2} \qquad (for\ rhombohedral\ structure) \qquad (3.4)$$

$$\frac{1}{d^2} = \frac{h^2}{a^2} + \frac{k^2}{b^2} + \frac{l^2}{c^2} \qquad (for\ orthorhombic\ structure) \qquad (3.5)$$

Where $d=\lambda/2sin\theta$ ($\lambda=1.54$)

The obtained values have been summarized in the Table3.1.

Table 3.1 Values of lattice parameters,volume and crystallite sizes of synthesized samples.

SAMPLE	a (Å)	b (Å)	c (Å)	VOLUME $(Å)^3$	STRUCTURE	CRYSTALLITE SIZE(nm)
BFO	5.57	5.57	13.921	373.99	Rhombohedral	46.2
Eu-BFO(450°C)	5.519	5.55	7.841	239.75	Orthorhombic	34.65
Eu-BFO(550°C)	5.539	5.56	7.851	241.23	Orthorhombic	39.6
Eu-BFO(650°C)	5.540	5.57	7.845	242.07	Orthorhombic	43.31

3.2 MICROSTRUCTURAL ANALYSIS:

Fig.3.2(a)-(c) show the variation of microstructure and average grain size amongst all the nanoparticles. Agglomeration of particles is witnessed which is possibly due to high surface energy of the nanoparticles[20]. All the synthesized nanoparticles have well defined grain boundaries. Eu doping influences the BFO sample as the particle agglomeration increases in doped sample. Further, we observe that increase in calcination temperature alters the particle size. With increase in calcination temperature, the particle size also increases which is in co ordination with the results of XRD. Smaller size grains observed at 450 °C expand as the calcination temperature increased to 650 °C.

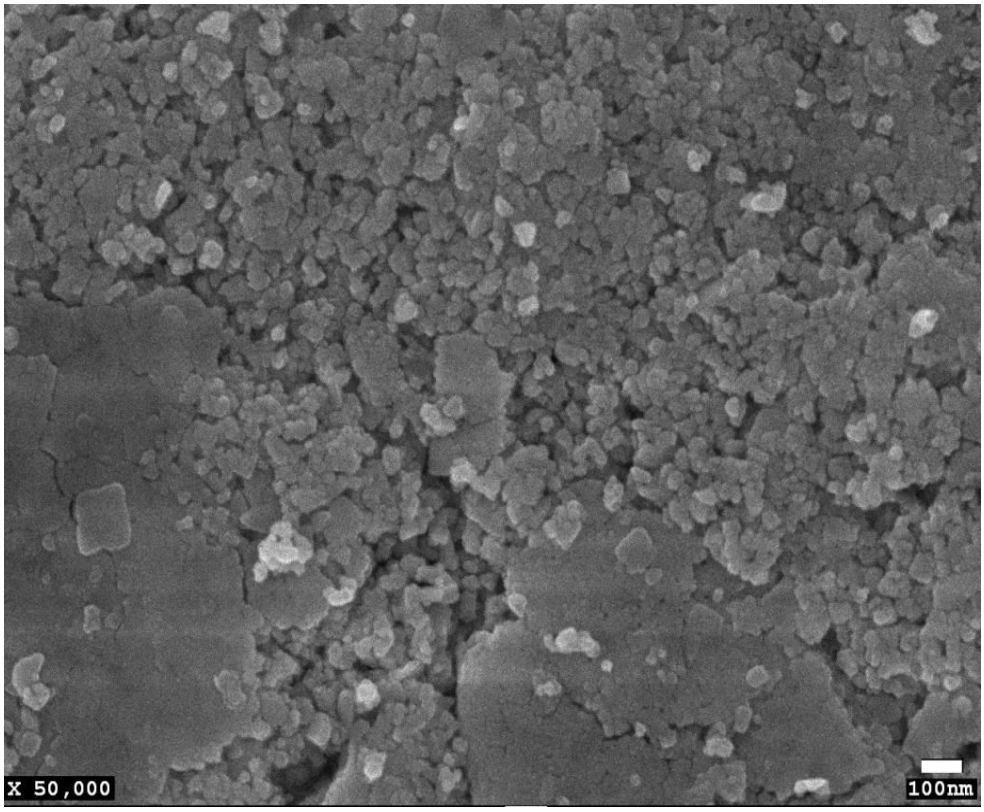

Fig.3.2(a) FE-SEM image of BFO

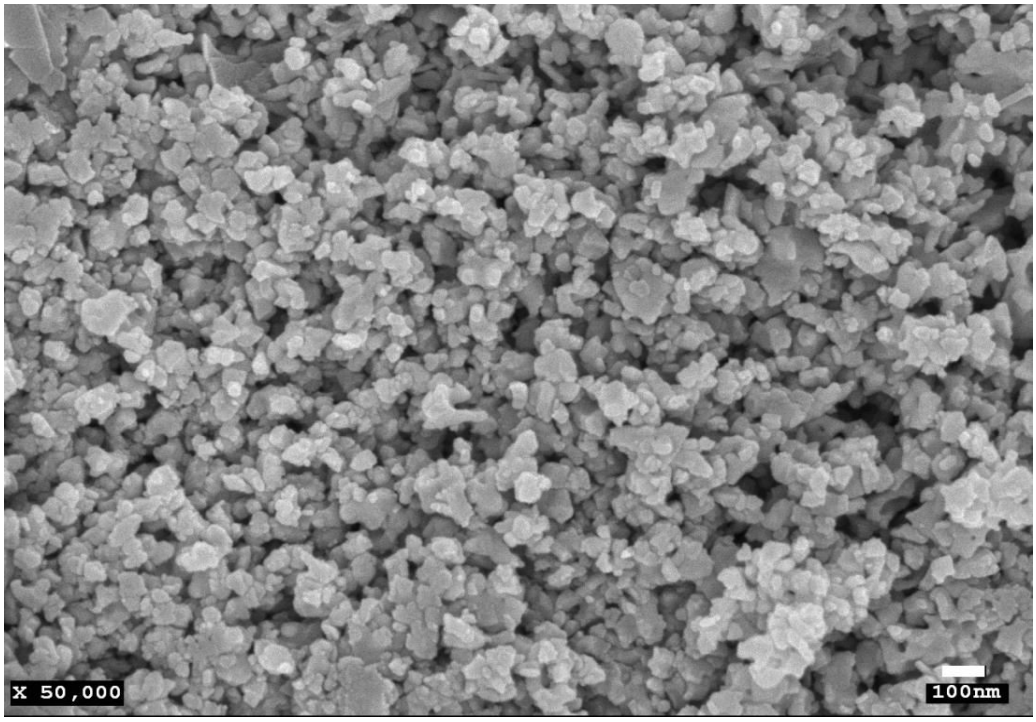

Fig3.2(b) FE-SEM image of Eu-BFO(450°C)

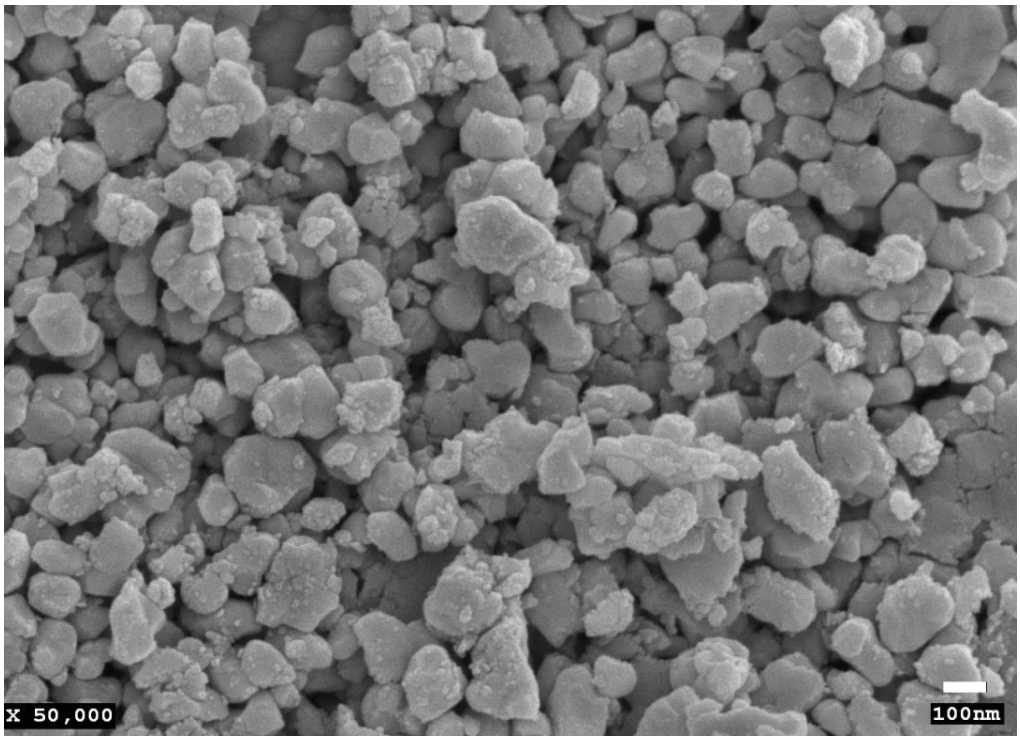

Fig.3.2(c) FE-SEM image of Eu-BFO(650°)C

It has been observed that the average grain size of Europium substituted nanoparticles increases from ~53nm to ~110nm with increase in calcination temperature from 450°C to 650°C respectively.

3.3 MAGNETIC PROPERTIES:

Room temperature M-H curves of pure BFO, Eu-BFO(450°C),Eu-BFO(550°C) and Eu-BFO(650°C) nanoparticles are shown in fig.3.3(a)

All the synthesized nanoparticles show ferromagnetism which goes well with previous rare earth doped bismuth ferrite reports[14,18,20].Firstly, with the Europium doping magnetization is enhanced. An increase in saturation magnetization from 3.62emu/g to 4.02emu/g is observed with Eu^{3+} ions doping. The magnetization is found to depend on particle size. With increase in size of particles, the ratio of surface to volume decreases and similar behaviour is shown by the antiferromagnetic spins present over the surface[20].

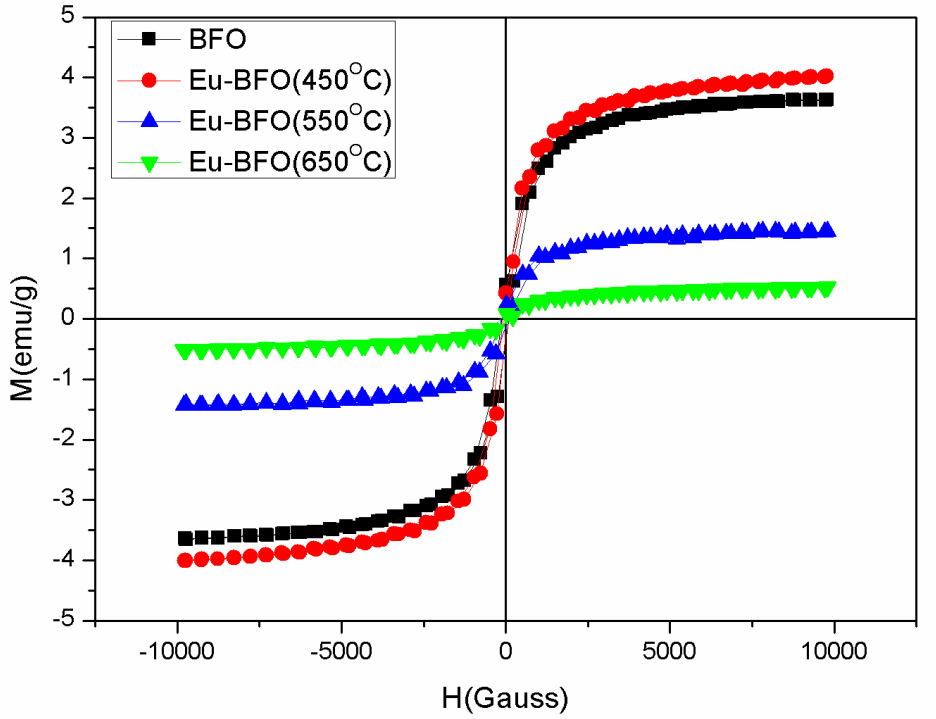

Fig. 3.3(a) M-H loops of the synthesized nanoparticles at various calcination temperatures.

The values of exchange bias field can been calculated by using the formula:

$$H_{eb} = (H_{C1}-H_{C2})/2 \qquad (3.6)$$

Where H_{C1} is the positive coercive field and H_{C2} is the negative coercive field. Coupling between ferromagnetic surface and antiferromagnetic core leads to the shift in hysteresis loop[28,29].

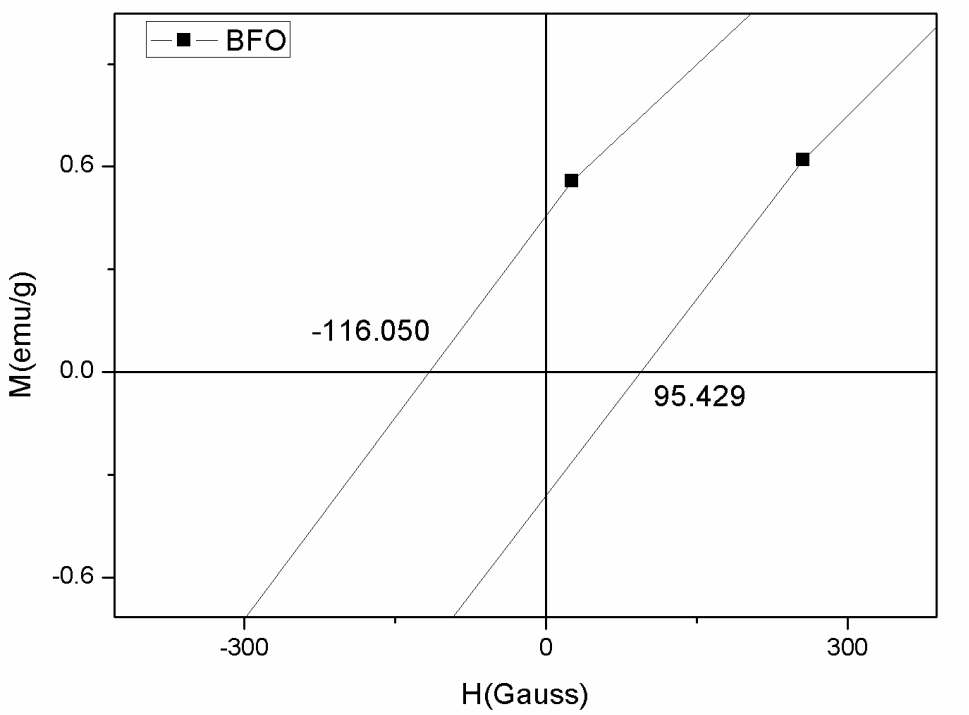

Fig.3.3(b) Enlarged view of M-H hysteresis loop of BFO with positive and negative coerecive fields.

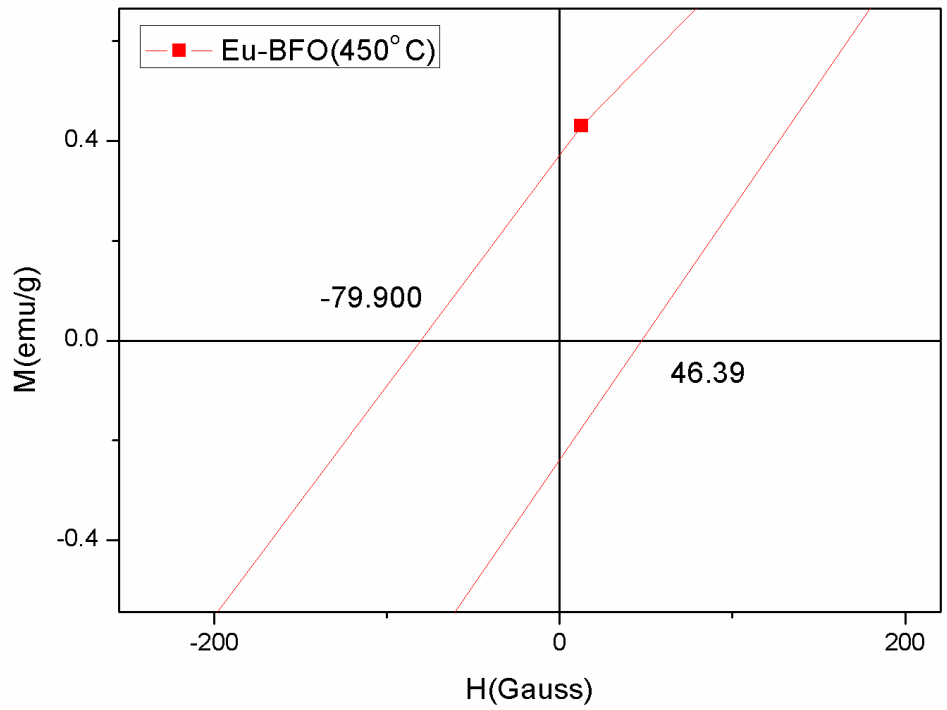

Fig.3.3(c) Enlarged view of M-H hysteresis loop of Eu-BFO(450°C) with positive and negative coerecive fields.

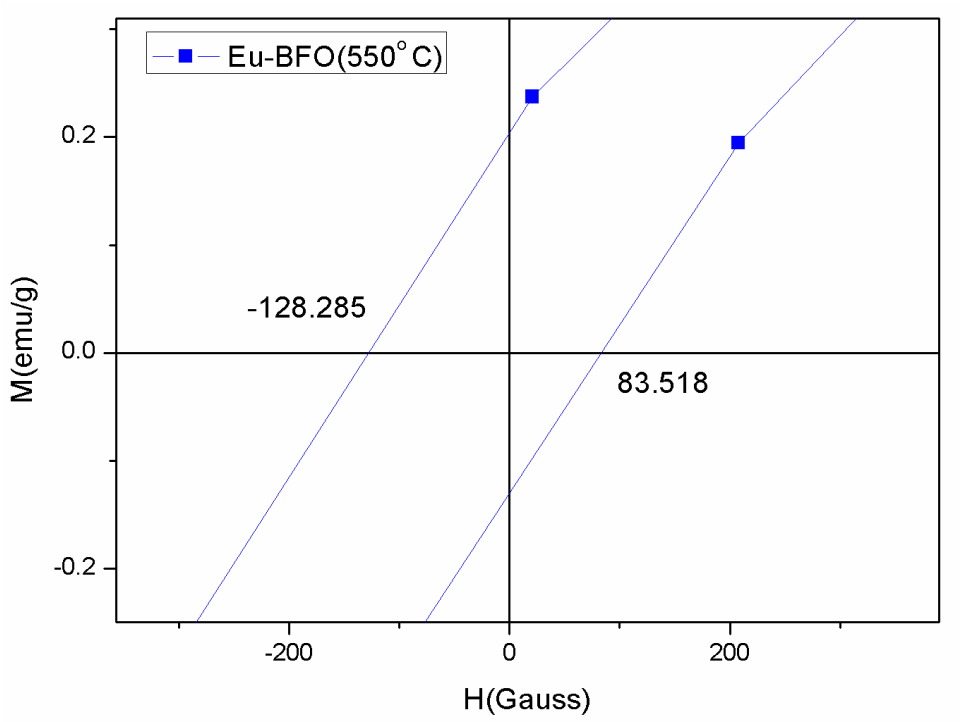

Fig.3.3(d) Enlarged view of M-H hysteresis loop of Eu-BFO(550°C) with positive and negative coerecive fields.

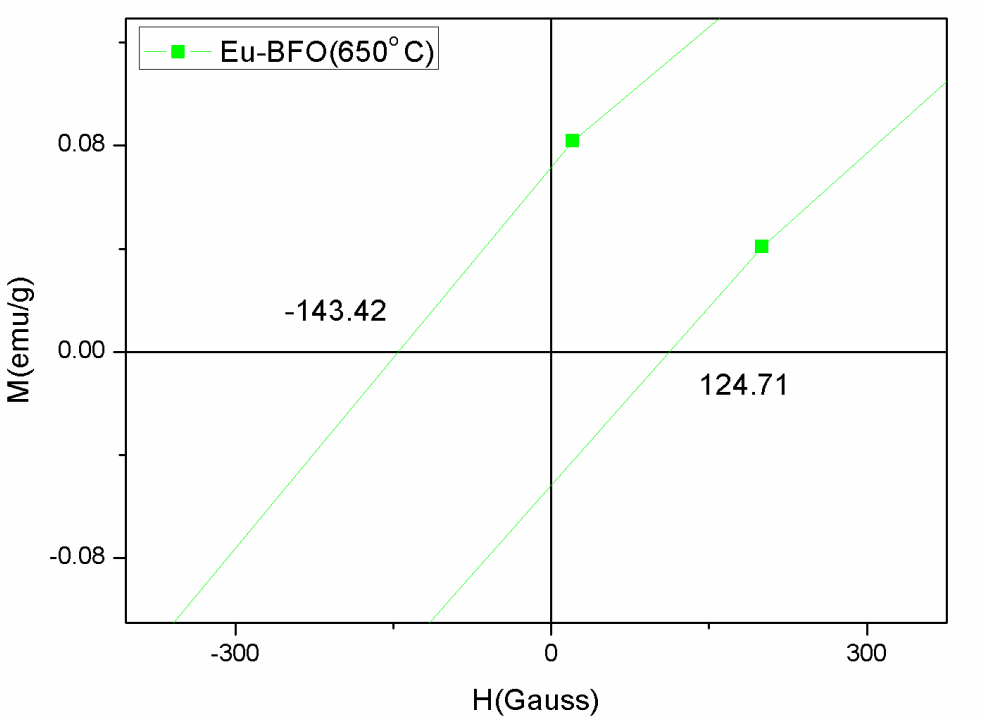

Fig.3.3(e) Enlarged view of M-H hysteresis loop of Eu-BFO(650°C) with positive and negative coerecive fields.

The values obtained for saturation magnetization and remanent magnetization are listed in table 3.2.

Table 3.2 Calculated Values of M_s,H_{eb},M_r of synthesized nanoparticles

Sample	**Saturation magnetization (M_s)(emu/g)**	**Remanent magnetization (M_r)(emu/g)**
BFO	3.62	0.04
Eu-BFO (450°C)	4.027	0.06
Eu-BFO (550°C)	1.438	0.03
Eu-BFO (650°C)	0.511	0.01

3.4 DIELECTRIC ANALYSIS:

The frequency dependent behaviour of permittivity for BFO, Eu-BFO(450°C),Eu-BFO(650°C) at room temperature is shown in the fig.3.4(a).

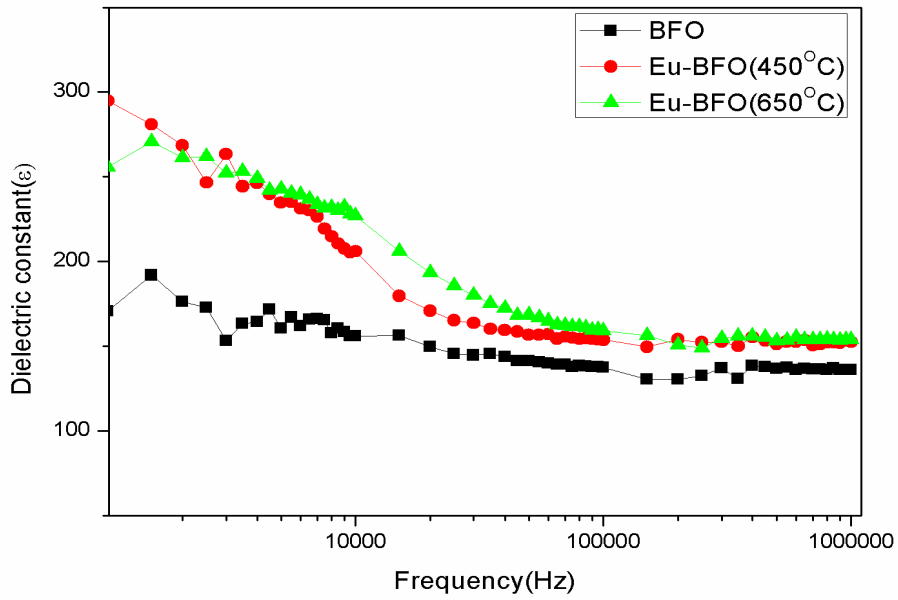

Fig.3.4(a) Frequency dependence plot of dielectric constant

Doping of Eu^{3+} ions in $BiFeO_3$ increases the value of dielectric constant. This may be due to the structural distortions produced in BFO with Eu^{3+} ions doping[30]. It is observed that particle size plays has a huge effect on the dielectric constant of the nanoparticles. A decrease in value of dielectric constant has been observed with increase in particle size of Eu doped

$BiFeO_3$ nanoparticles. This is possibly due to the existence of nanosize grains in the synthesized samples which act as insulating barriers [30]. With increase in frquency, the values of dielectric constant in the synthesized samples decrease. This is so because at higher frequencies only electronic polarization contribution is taken into account [29]. Therefore, at high frequencies dielectric constant decreases.

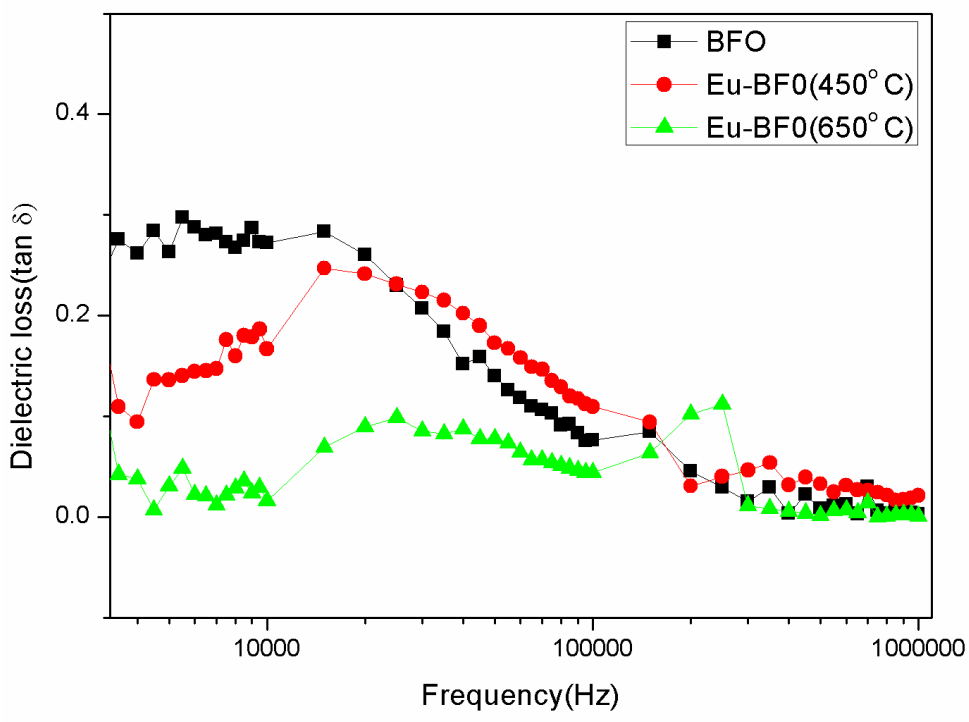

Fig.3.4(b) Dielectric loss of BFO, Eu-BFO(450°C),Eu-BFO(650°C)

Fig. 3.4(b) shows the variation of dielectric loss with frequency. A peak is observed in dielectric loss because of the resonance where the hopping frequency is approximately equal to that of the externally applied electric field. The dielectric loss is found to decrease with Eu doping. This observed decrease in dielectric loss could be ascribed to lowering of grain size.

Conclusion

A study of combined effect of doping and particle size on $Bi_{(1-x)}Eu_xFeO_3$ (x=0,0.15) nanoparticles synthesized by sol gel method has been reported. Structural transformation from rhombohedral to orthorhombic has been observed with Europium doping at x=0.15. Eu^{3+} substitution reduced the particle size whereas by increasing the calcination temperature(550°C-650°C)increased the particle size. Enhancement in magnetic property has been observed with maximum magnetization value of 4.02emu/g. Europium doping improved dielectric parameters with reduction in dissipation factor. Hence, from these observations we conclude that elemental substitution is an effective way to enhance the magnetic and dielectric properties of $BiFeO_3$.

References:

1. N.A. Spaldin, S.W. Cheong and R.Ramesh, Physics Today, 63,38(2010).

2. S. Picozzi and C. Ederer, Journal of Physics:Condensed Matter, 21,303(2009).

3. B.B. Van Aken, T.T. Palstra, A. Filippetti and N.A. Spaldin, Nature materials, 3,1639 (2004).

4. T. Kimura, T. Goto, H. Shintani and K. Ishizaka, Nature, 426,55(2003).

5. N. Hur, S. Park, P.A. Sharma, J.S. Ahn, S. Guha and S. W. Cheong, Nature, 429,392 (2004).

6. G. Catalan and J.F. Scott, Advanced Materials, 26,2463(2009).

7. A.K. Zvezdin, A.S. Logginov, G.A. Meshkov and A.P. Pyatakov, Bulletin of the Russian Academy of Sciences: Physics, 71,1561(2007).

8. Z. Hu, M. Li, Y. Yu, J. Liu, L. Pei, J. Wang, X. Liu, B. Yu and X. Zhao, Solid State Communications, 150,1088(2010).

9. T.J. Park, G.C. Papaefthymiou, A.J. Viescas, A.R. Moodenbaugh and S.S. Wong, Nano Letters, 7,766(2007).

10. S.M. Selbach, T. Tybell, M.A. Einarsrud and T. Grande, Chemistry of Materials, 19,6478(2007).

11. S. Goswami, D. Bhattacharya and P. Choudhury, The Journal of Applied Physics, 109, 07D737(2011).

12. A. Jaiswal, R. Das, K. Vivekanand, P.M. Abraham, S. Adyanthaya and P. Poddar, The Journal of Physical Chemistry,114,2108(2010).

13. R. Mazumder, S. Ghosh, P. Mondal, D. Bhattacharya and S. Dasgupta, The Journal of Applied Physics, 100,033908(2006).

14. G. Dhir, P. Uniyal and N.K. Verma, Journal of Materials Science:Materials in Electronics, 26,3538(2015).

15. M. Hasan, M.A. Hakim, M.A. Basith, M.S. Hossain, B. Ahmmad, M.A. Zubair, A. Hussain and M.F. Islam, American Institute Of Physics Advances, 6,035314(2016).

16. M. Kaur and P. Uniyal, Journal of Superconductivity and Novel Magnetism 2,431(2016).

17. Z.M. Tian, S. L. Yuan, X. L. Wang, X. F. Zheng, S. Y. Yin, C. H. Wang, and L. Liu, The Journal of Applied Physics, 106,103912(2009).

18. J. Liu, L. Fang, F. Zheng, S. Ju and M. Shen, Applied Physics Letters, 13,022511(2009).

19. S. Chauhan, M. Kumar and S.C. Katyal, American Institute of Physics Publishing, 1731,130029(2016).

20. G. Dhir, P. Uniyal and N.K. Verma, Journal of Superconductivity & Novel Magnetism, 27,2621(2014).

21. W. Meng, R. Hu, J. Yang, Y. Du, J. Li and H. Wang, Chinese Journal of Catalysis, 31,1283(2016).

22. D. Jalandhara, G. Singh and K. Yadav, American Institute of Physics Publishing, 1728,020437 (2016).

23. H. Yan, H. Deng, N. Ding, J. He, L. Peng, L. Sun, P. Yang and J. Chu, Materials Letters, 111,123(2013).

24. K.S. Nalwa and A. Garg, The Journal of Applied Physics, 103,044101(2008).

25. Z. Hu, M. Li, J. Liu, L. Pei, J. Wang, B. Yu and X. Zhao, The Journal of the American Ceramic Society, 93,2743(2010).

26. B. Bhushan, A. Basumallick, S.K. Bandopadhyay, N.Y. Vasanthacharya and D. Das, The Journal of Applied Physics, 42,065004(2009).

27. G. Singla, K. Singh and O.P. Pandey, The Journal of Applied Physics, 113,237(2013).

28. B. Bhushan, Z. Wang, J. Tol, N.S. Dalal, A. Basumallick, N.Y. Vasanthacharya, S. Kumar and D. Das, Journal of American Ceramic Society,95,1985(2012).

29. R. Das, T. Sarkar and K. Mandal, The Journal of Applied Phyics, 45,455002(2012).

30. G. Dhir, G. S. Lotey, P. Uniyal and N. K. Verma, Journal of Materials Science: Materials in Electronics, 24,4386(2013).